

## Article

# A Thermal Hydrodynamic Model for Emulsified Oil-Lubricated Tilting-Pad Thrust Bearings

Wu Ouyang<sup>1,2,3</sup>, Ziyang Yan<sup>4</sup>, Xincong Zhou<sup>1,2,3</sup>, Bin Luo<sup>5</sup>, Bin Wang<sup>3,4</sup> and Jian Huang<sup>2,3,\*</sup>

<sup>1</sup> State Key Laboratory of Maritime Technology and Safety, Wuhan University of Technology, Wuhan 430063, China; ouyangw@whut.edu.cn (W.O.); xczhou@whut.edu.cn (X.Z.)

<sup>2</sup> School of Transportation and Logistics Engineering, Wuhan University of Technology, Wuhan 430063, China

<sup>3</sup> Reliability Engineering Institute, National Engineering Research Center for Water Transport Safety, Wuhan 430063, China; wangbinpluto@whut.edu.cn

<sup>4</sup> School of Naval Architecture, Ocean and Energy Power Engineering, Wuhan University of Technology, Wuhan 430063, China; yan\_zi\_y@whut.edu.cn

<sup>5</sup> China Ship Development and Design Center, Wuhan 430064, China; luonaerbin@163.com

\* Correspondence: huangfeihong@whut.edu.cn; Tel.: +86-1366-716-2352

**Abstract:** On maritime vessels, external factors such as explosions, collisions, and grounding can cause the emulsification of lubricating oil by seawater pollution, which can affect the lubrication of a ship's thrust bearing. To explore the influence of the mixed emulsification of lubricating oil and seawater on the lubrication performance of thrust bearings, this study conducted an emulsification experiment, from which the viscosity equation of the oil–water mixture was obtained. A thermal hydrodynamic model (THD) of bearings considering oil–water mixed emulsification was established, and the Finite Difference Method (FDM) was used for analysis. The results show that according to the characteristics of the manifold, the mixture is divided into water-in-oil (W/O) and oil-in-water (O/W). In the W/O flow with higher viscosity, the film thickness becomes higher, but the power loss increases. In the O/W manifold with low viscosity, the thin film easily causes mixed friction. In the demulsification stage of the mixed liquid, the thickness loss of the film is huge, and the collision between the thrust-bearing pad and the inference plate may cause the pad to be ablated. The influence of specific heat capacity on temperature is greater than the temperature rise caused by viscosity.

**Keywords:** tilting-pad thrust bearing; emulsification; viscosity; thermal conduction



**Citation:** Ouyang, W.; Yan, Z.; Zhou, X.; Luo, B.; Wang, B.; Huang, J. A Thermal Hydrodynamic Model for Emulsified Oil-Lubricated Tilting-Pad Thrust Bearings. *Lubricants* **2023**, *11*, 529. <https://doi.org/10.3390/lubricants11120529>

Received: 31 October 2023

Revised: 3 December 2023

Accepted: 8 December 2023

Published: 13 December 2023



**Copyright:** © 2023 by the authors. Licensee MDPI, Basel, Switzerland. This article is an open access article distributed under the terms and conditions of the Creative Commons Attribution (CC BY) license (<https://creativecommons.org/licenses/by/4.0/>).

## 1. Introduction

The quality of lubricating oil determines lubrication performance of a ship thrust bearing. Lubricating oil pollution will directly affect the lubrication state of the thrust bearing, increase the power consumption of shafting, and even lead to damage to the bearing pad [1,2]. Water is one of the common sources of oil pollution [3]. Many factors cause water pollution of ship lubricating oil. For example, in the marine environment, water often condenses and penetrates the oil tank holes into the ship lubricating oil [4]. In addition, damage to the lubricating oil tank and the increase in shaft seal gap caused by external risk factors such as explosion, collision, and grounding while in service will also lead to seawater entering the lubricating oil system, resulting in lubricating oil pollution [5]. Many scholars have studied bearing water pollution. H. Hamaguchi et al. [6] found that the hydrodynamic lubrication state of water-in-oil (W/O) emulsion is almost entirely determined by the characteristics of pure oil, and it is difficult to generate hydrodynamic lubrication for oil-in-water (O/W) emulsion. Zhang F et al. [7] directly observed the characterization of micro-sized water-in-oil emulsion in the EHL point contact area via high-speed camera, and explained the critical conditions of water-in-oil emulsification affecting EHL contact. Hili J [8] used fluorescence and infrared microscopy techniques to study contact lubrication under oil-in-water conditions. The oil-in-water mixture showed

a stratified state at low speeds and a gradient distribution at high speeds. Soltanahmadi et al. [9] and Haque et al. [1,10] studied the induction behavior of water in lubricating oil on the white etching cracking of a bearing pad, and proved the damage caused to alloy bearings by water in terms of friction and wear. Studies have shown that a small amount of water pollution does not change bearing lubrication characteristics. Liu H et al. [11] found that the ratio of seawater mixed in the radial bearing lubricating oil can be increased from 0.5% to 3%. Elias [4,12] fitted the mixed-viscosity model with a moisture content of 0–10%, studied the performance of the thrust bearing under 7% moisture content, and proved that the thrust bearing can be applied to lubricating oil with low moisture content. At present, the research on the emulsification and lubrication of thrust bearings only focuses on a small amount of water pollution. However, if a ship sustains damage at sea, (and the amount of oil mixed with seawater can be high in such an event), the ship needs to be able to return to port. There are few studies on the lubrication performance of thrust bearings in high moisture oil–water mixtures.

Combined with the above literature, considering that water pollution will lead to a change in such physical parameters as the viscosity, density, and specific heat of lubricating oil, it is very important to determine these characteristics in relation to the emulsified viscosity of ship lubricating oil in order to study and predict the oil–water mixed lubrication state of the ship thrust bearing. The viscosity of the mixed liquid is usually related to its manifold [13]. Different types of lubricating oil, moisture content, temperature, stirring speed, and salt content will produce different manifolds. According to the flow form of the oil–water mixture, it can be divided into oil-in-water (O/W) and water-in-oil (W/O) manifolds [14], in which oil and water exist in a continuous phase or a dispersed phase, respectively [15,16]. The process of converting an oil–water two-phase liquid is illustrated in Figure 1. When the moisture content in the oil–water mixture is low, the oil–water mixture will form small droplets under the action of high-speed stirring shear [17]. These droplets gradually disperse and condense during the movement, and finally achieve the dynamic balance [18]. The emulsification of the oil–water mixture forms a stable W/O manifold. Among them, asphaltenes, resins, hydrocarbons, and particulates in the lubricating oil will act as emulsifiers to promote the formation of an emulsion interface film to stabilize the emulsion structure [17]. When the moisture content in the mixed liquid reaches and exceeds the phase inversion point, enough dispersed droplets condense into a continuous phase transition under the action of motion and pad tension to cut off the original continuous phase into dispersed droplets, realizing the transformation of the manifold [14,19–22]. At this point, the O/W manifold is formed.

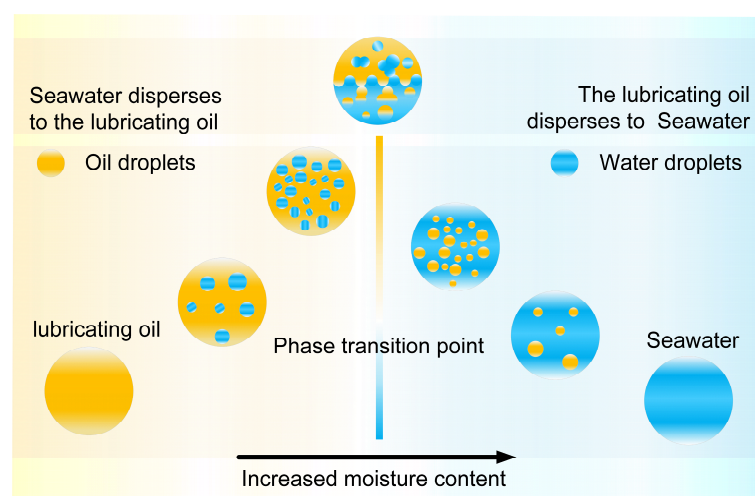


**Figure 1.** Oil–water two-phase hybrid phase transition diagram.

A large number of researchers have studied the emulsification model. Taylor proposed the two-phase concept, introduced the liquid–liquid phase dispersion analysis, and extended the viscosity prediction of Einstein’s model for ultra-low concentration rigid spherical particle suspensions [23]. Brinkman [24], Mooney [25], and Pal [26,27] modified the model by adding the concept of a demulsification point, and extended the application range of the ratio  $K$  of the dispersed phase to the continuous phase to 0.012–1170. In addition, Ronningsen [19], Walther [28], and Vogel [29] considered the shear rate, temperature, and other factors in the viscosity model. However, for ship lubricating oil and seawater, the oil–water mixed emulsification model considering temperature and moisture content is not clear.

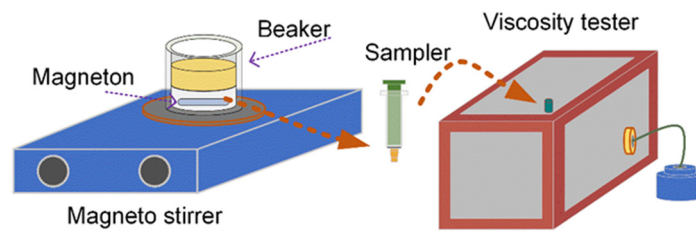
To find out the lubrication characteristics of thrust bearings after immersion in seawater for the oil system of a ship in distress, the establishment of a widely applicable prediction model of lubrication characteristics of oil-immersed emulsified thrust bearings is urgently needed.

For this paper, an emulsification viscosity characterization test of ship lubricating oil mixed with seawater was conducted. The viscosity equation considering 0–100% moisture content and 35–60 °C temperature was fitted. A THD bearing lubrication model considering the emulsification viscosity equation was established. The finite difference method (FDM) was used to calculate the bearing lubrication characteristics under different moisture content, and the influence of different degrees of seawater pollution on bearing lubrication was obtained from three aspects: film thickness, temperature, and pressure.

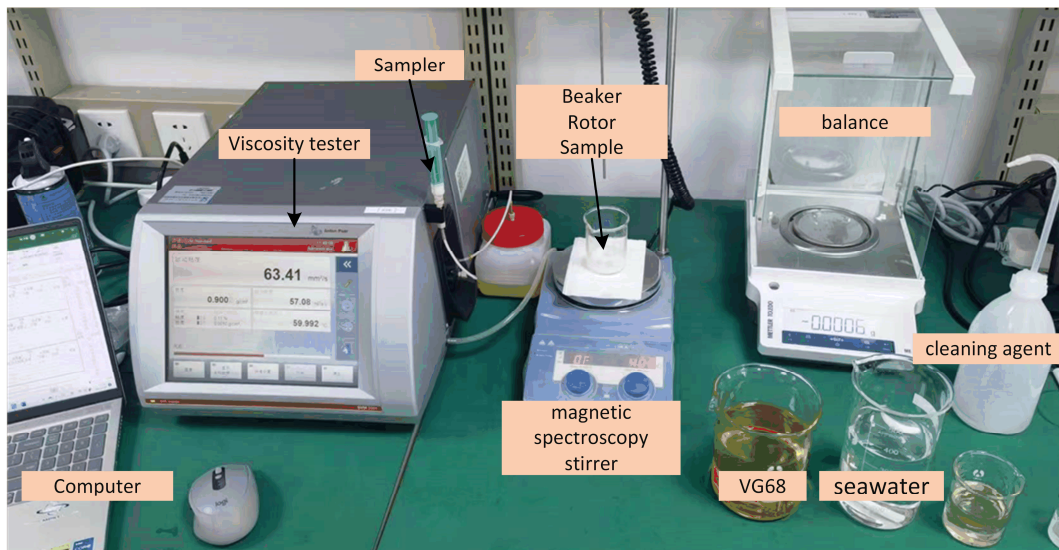
## 2. Emulsification Characterization of Lubricating Oil in Water

Figure 2 is the emulsification characterization experimental device diagram. An IKA RCT magnetic stirrer with a 50 mm rotor was used as the stirring device; the speed was set to 1150 r/min, and the stirring time was 5 min. A viscosity tester SVM2001 was used to test the dynamic viscosity of the sample (hereinafter referred to as viscosity). The sampling mode was set to repetition, and the results were obtained three times. The measurement accuracy was set as ‘fast’ (deviation  $\pm 0.25\%$ ), the test temperature range was 35–60 °C, and the step length was 5 °C. The commonly used lubricating oil VG68 and seawater simulated liquid [30] were selected as the basic test samples. At the ambient temperature of 27 °C, 11 groups of samples with moisture content of 0–100% were prepared using an ultramicrobalance with a 10% step size. The sample was stirred at room temperature for 5 min; after standing for 1 min, a 3 mL sample was placed into the SVM2001 viscosity tester to test the viscosity. The demulsification interval was found, the solution was configured according to the 1% step size to find the demulsification point, and the viscosity of the demulsification point was tested.

The test showed that the sample with a moisture content of 10–50% can form the W/O manifold, and the emulsion structure is stable under this manifold. The samples with a moisture content of 60–90% produced the O/W manifold, which was unstable, and stratification occurred after stirring stopped. The upper-half layer was emulsified oil, and the lower-half layer was emulsified water. In the demulsification range of 50–60% moisture content, a demulsification point of 54% at room temperature was found, and the stable viscosity value at 35 °C was only obtained due to the influence of temperature. In addition, as the moisture content increased beyond 54%, the continuous drip of the seawater simulation solution according to the step mass fraction of 1% still emulsified until the moisture content was 76%. However, the emulsification structure at this stage was unstable and its viscosity value could not be accurately measured, so it was not included in the viscosity data. The viscosity of the above samples in the demulsification section of the moisture content range of 50–60%, is shown in Figure 3.



(a) Diagram of the experimental device



(b) Actual experimental device

Figure 2. Emulsification characterization experimental device.

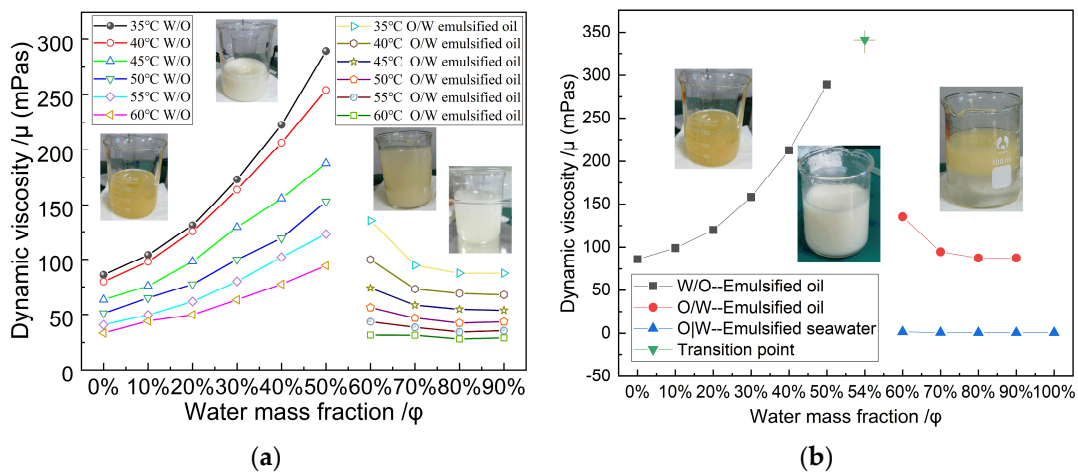


Figure 3. Characterizing two-phase liquid emulsification at global moisture ratio: (a) viscosity-temperature relationship of oil emulsions with different moisture contents; (b) emulsified oil, emulsified seawater, and phase point viscosity plots at 35 °C.

Figure 3 is a global two-phase liquid emulsification characterization diagram. Figure 3a shows the W/O manifold viscosity values of the samples with 0% moisture content, and the samples with 10–90% moisture content between 35 °C and 60 °C. When the moisture content is in the range of 0–50%, the transparency of the emulsion decreases with the increase in moisture content until it is milky white. The viscosity of the sample increases with the increase in moisture content, and the higher the temperature, the smaller the viscosity increase amplitude. When the moisture content is in the range of 60–100%, the transparency

of the W/O manifold sample decreases with the increase in moisture content; the viscosity of the emulsion decreases with the increase in moisture content and decreases sharply compared with the viscosity value of 50% moisture content. This is due to the large number of small water droplets in the oil phase after demulsification. These condense into large water droplets and destroy the original emulsion interface film, affected by the density difference and poor settlement, resulting in a significant reduction in moisture content in the W/O manifold sample. Figure 3b records the viscosity value of the sample at 35 °C when the moisture content is 0–100% (10% step) and 54%. When the moisture content of the sample is 0–50%, the viscosity of the emulsion increases from 86.04 mPas to 288.3 mPas with the increase in moisture content. The oil in this interval is a continuous phase, and the seawater is dispersed in the oil in the form of small droplets, which increases the liquid viscosity. When the moisture content is 50–60%, with the increase in moisture content the viscosity reaches the highest (346.87 mPas) when the moisture content is 54%. After increasing the moisture content by 1%, the sample manifold is converted from W/O to O/W. The sample gradually changes to transparent from milky white, and the liquid level in the beaker increases instantaneously, which indicates that the liquid viscosity in the beaker drops sharply. When the moisture content is 60–90%, with the increase in moisture content, the transparency of the sample increases and obvious stratification occurs after standing. The turbidity of the stratified emulsified liquid gradually decreases, the viscosity of emulsified oil decreases from 135.4 mPas to 87.43 mPas, and the viscosity of emulsified seawater decreases from 1.76 mPas to 0.77 mPas.

### 3. Thermo-Hydrodynamic Model Considering Oil–Water Mixed Emulsification

#### 3.1. Viscosity–Temperature Equation

The Walther [28] and Vogel [29] models are well-known viscosity–temperature models, as shown in Equations (1) and (2):

$$\ln \ln(\mu + 0.7) = n + m \ln(t + 273.15) \quad (1)$$

$$\mu = Ae^{\frac{B}{t+C}} \quad (2)$$

where  $\mu$  is the dynamic viscosity, mPas;  $t$ , the temperature, °C;  $m$ ,  $n$  is the viscosity parameters of Walther's model; and  $A$ ,  $B$ , and  $C$  are the viscosity parameters of Vogel's model.

To establish the thermal–hydrodynamic (THD) model of thrust bearing with oil–water mixed emulsification, it was necessary to accurately fit the experimental results of emulsification characterization to obtain the viscosity–temperature equation of mixed fluid under different moisture.

The viscosity test results of lubricating oil VG68 and seawater are brought into the model to obtain the fitting equation, as shown in Figure 4.

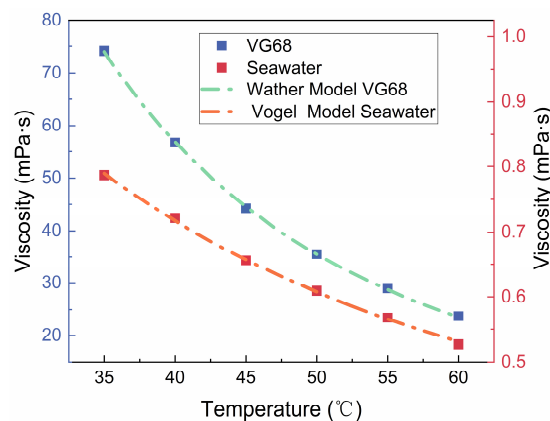


Figure 4. Viscosity–Temperature of VG68 versus seawater.

In Figure 4, VG68 is more consistent with the Walther model, and the seawater is more consistent with the Vogle model. Following the fit, the viscosity parameters of lubricating oil are  $m = 24.09$  and  $n = -3.947$ , and the viscosity parameters of seawater are  $A = 0.0767$ ,  $B = 293.0$ , and  $C = 86.54$ .

In the state of a W/O emulsion, the fluid mixture remains stable, with the lube oil serving as the continuous phase. Therefore, taking into account the viscosity–temperature characteristics of the lubricating oil, we can make an extension. Considering that the emulsified oil is a W/O manifold, the ‘ $n$ ’ term in Equation (1) is extended, and the empirical Equation (3) satisfying different moisture content is obtained by fitting the experimental data:

$$\ln \ln(\mu + 0.7) = n + m \ln(t + 273.15) + \ln(1 + c_1\varphi + c_2\varphi^2) \quad (3)$$

where  $c_1$  and  $c_2$  are the moisture viscosity parameters.

The parameter values applicable to the test results in Equation (3) are  $A = 24.09$ ,  $B = -3.947$ ,  $c_1 = 0.3691$ , and  $c_2 = 0.4090$ .

The structure of the mixture under the oil-in-water manifold is unstable, and the viscosity cannot be accurately measured using the existing equipment. Therefore, the viscosity calculations for the O/W emulsion state were performed using Equation (4) as described in the mixing model [31]:

$$\left\{ \begin{array}{l} \mu_r \left( \frac{2\mu_r + 5K}{2 + 5K} \right)^{\frac{3}{2}} = \left( 1 - \frac{\varphi}{1 - c\varphi} \right)^{-\frac{5}{2}} \\ K = \frac{\mu_d}{\mu_c} \\ c = \frac{1}{1 - \varphi_c} \\ \mu(\varphi) = \mu_r \mu_c \\ \mu_c = A \frac{B}{e^{t+C}} \end{array} \right. \quad (4)$$

where  $\mu_c$  represents the viscosity of the continuous phase, mPas;  $\mu_d$ , the viscosity of the dispersed phase, mPas;  $\varphi_c$ , the moisture content of turning point; and  $\mu_r$ , viscosity ratio after mixing.

Based on the above four viscosity models, the global oil–water mixed emulsification model with 0–100% moisture content is shown in Figure 5. In the figure, the mass fraction of water as the dispersed phase in the W/O manifold is 0–50%, and the mass fraction of oil as the dispersed phase in the O/W manifold is 0–40%. It can be seen that the viscosity of the mixture increases with the increase in the proportion of the dispersed phase in the respective manifold. In the range of 50–60% moisture content, the mixed liquid manifold changes from W/O to O/W, and the viscosity changes sharply. The sharp decrease in viscosity may change the lubrication state, which leads to damage to the bearing pad. However, the viscosity ratio of the mixed liquid decreases from 40.1 to 9.8 with the increase in temperature in the phase transition interval, which is affected by the increase in the internal energy of the mixed liquid molecules after the temperature increases. The thermal motion of the molecules increases and the spacing increases, which shows that the viscosity decreases. The dispersed phase in the moisture range of 60–100% is seawater. When the temperature is 35 °C, the viscosity increases from 0.76 to 7.53 mPas with the increase in lubricating oil content.

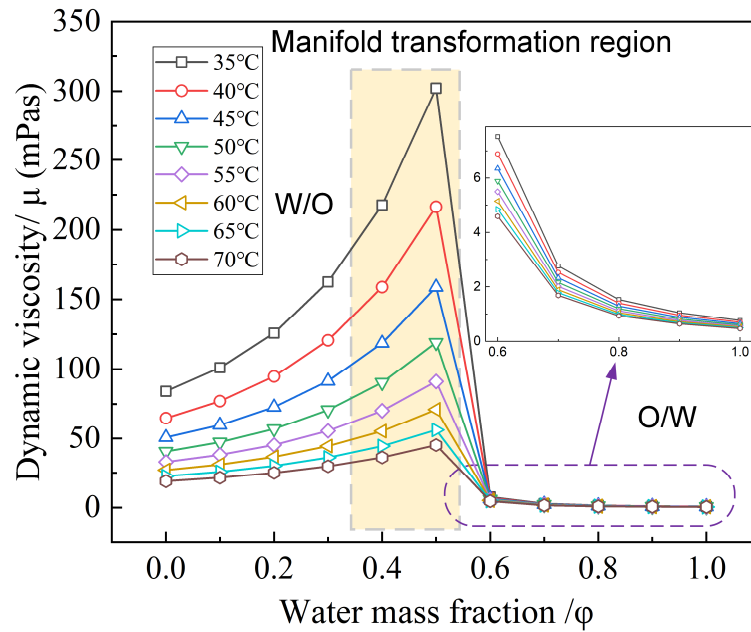


Figure 5. Global moisture content viscosity.

3.2. Governing Equations

A THD model of tilting-pad thrust bearing was constructed, including the Reynolds equation, film thickness equation, temperature equation, and viscosity–temperature equation. Assuming that the bearing works in a steady state, Figure 6 shows the structural parameters of the bearing. The liner tilts around its fulcrum in both radial and circumferential directions during movement. When the torque on the bearing pad is balanced, a wedge-shaped film is formed between the bearing and the plate.

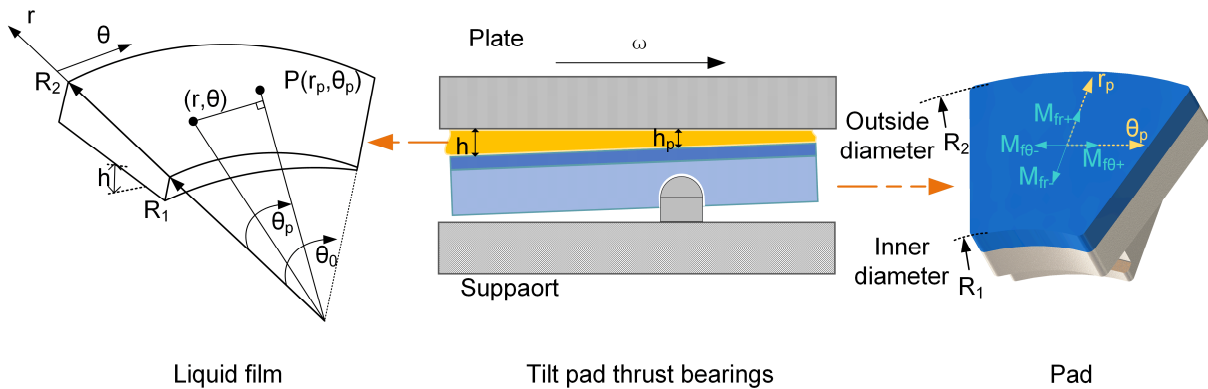


Figure 6. Structure of the bearing.

In this state, the film thickness equation at any point in the cylindrical coordinate system  $(r, \theta)$  is determined:

$$h(r, \theta) = h_p + \gamma_r[r \sin(\theta_p - \theta)] + \gamma_\theta[r \cos(\theta_p - \theta) - r_p] \tag{5}$$

where  $h_p$  represents the film thickness at the pivot;  $\theta_p$ , the pivot angle;  $r_p$ , the pivot radius;  $\gamma_r$ , the radial tilt angle; and  $\gamma_\theta$ , the circumferential tilt angle.

Under the assumption of incompressible fluid, in the two-dimensional case, the Reynolds equation can be expressed as follows:

$$\frac{\partial}{\partial r} \left( \frac{rh^3}{\mu} \frac{\partial p}{\partial r} \right) + \frac{1}{r} \frac{\partial}{\partial \theta} \left( \frac{h^3}{\mu} \frac{\partial p}{\partial \theta} \right) = 6r\omega \frac{\partial h}{\partial \theta} \tag{6}$$

where  $\mu$  is the dynamic viscosity;  $h$ , the film thickness; and  $\omega$ , the angular velocity. The boundary condition is:

$$\left. \frac{\partial p}{\partial \theta} \right|_{\Gamma_1} = 0, \quad p|_{\Gamma} = 0 \quad (7)$$

where  $\Gamma_1$ , the film rupture boundary; and  $\Gamma$ , the film periphery boundary.

The energy equation considering the axial heat transfer is:

$$\rho C_p \left[ \left( \frac{\omega r h}{2} - \frac{h^3}{12\mu} \frac{1}{r} \frac{\partial p}{\partial \theta} \right) \frac{1}{r} \frac{\partial t}{\partial \theta} - \frac{h^3}{12\mu} \frac{\partial p}{\partial r} \frac{\partial t}{\partial r} \right] = k \frac{\partial^2 T}{\partial z^2} + \frac{\mu \omega^2 r^2}{h} + \frac{h^3}{12\mu} \left[ \left( \frac{\partial p}{\partial r} \right)^2 + \left( \frac{1}{r} \frac{\partial p}{\partial \theta} \right)^2 \right] \quad (8)$$

where  $\rho$  is density, Kg/m<sup>3</sup>;  $C_p$ , specific heat at constant pressure, J/(kg·°C); and  $k$ , the heat transfer coefficient, W/(m·K); the boundary condition is:

$$\left\{ \begin{array}{l} t = t_{in} \\ r = R_2 \\ \frac{\partial t}{\partial r} = 0 \end{array} \right\} \quad (9)$$

The heat transfer equation considering the heat conduction on the pad of the pad is:

$$\frac{1}{r} \frac{\partial}{\partial r} \left( r \frac{\partial T}{\partial r} \right) + \frac{1}{r^2} \frac{\partial^2 T}{\partial \theta^2} + \frac{\partial^2 T}{\partial z^2} = 0 \quad (10)$$

The boundary condition is:

$$\left\{ \begin{array}{l} -k \frac{\partial T}{\partial n} = \lambda \Delta T \\ k \frac{\partial T}{\partial z} = k_b \frac{\partial T_b}{\partial z} \end{array} \right\} \quad (11)$$

where  $\lambda$  is the convection coefficient, W/(m<sup>2</sup>·K);  $\Delta T$ , solid-liquid boundary temperature difference, °C;  $k_b$ , the boundary heat transfer coefficient, W/(m·K); and  $T_b$ , the boundary temperature, °C.

Density and specific heat are linearly related after mixing [32,33]:

$$\left\{ \begin{array}{l} \rho_{mix} = \varphi \rho_{seawater} + (1 - \varphi) \rho_{oil} \\ C_{mix} = \varphi C_{seawater} + (1 - \varphi) C_{oil} \end{array} \right\} \quad (12)$$

### 3.3. Simulation Method

Combined with the two-phase mixing theory, the thermal–hydrodynamic lubrication (THD) model of thrust bearing under oil–water mixed emulsification is established. The mesh density is set to 21 × 21, and the convergence criteria are as follows:

the pressure convergence criteria is:

$$E_p = \frac{\sum_i |p_i^{n+1} - p_i^n|}{\sum_i |p_i^{n+1}|} \leq 10^{-6} \quad (13)$$

the temperature convergence criteria is:

$$E_T = \frac{\sum_i |T_i^{n-1} - T_i^n|}{\sum_i |T_i^{n+1}|} \leq 10^{-6} \quad (14)$$

the force criteria is:

$$E_F = |F_f - F_0| \leq 10^{-6} \quad (15)$$

where  $F_f$  is the iterative pressure and  $F_0$  is the loading force.

The Moment criteria is:

$$E_N = \left( M_{fr}^2 + M_{f\theta}^2 \right)^{\frac{1}{2}} \leq 10^{-6} \tag{16}$$

where  $M_{fr}$  is the radial direction torque and  $M_{f\theta}$  is the circumferential direction torque.

The Finite Difference Method (FDM) [34–37] is used to solve the model, and the calculation process is shown in Figure 7. The initial parameters are input, and the viscosity; pad deformation; initial oil film thickness; and oil film pressure are calculated to achieve convergence. By adjusting the radial and circumferential inclination angles of the pad, the oil film bearing capacity and torque are balanced, and the oil film temperature is calculated to achieve convergence.

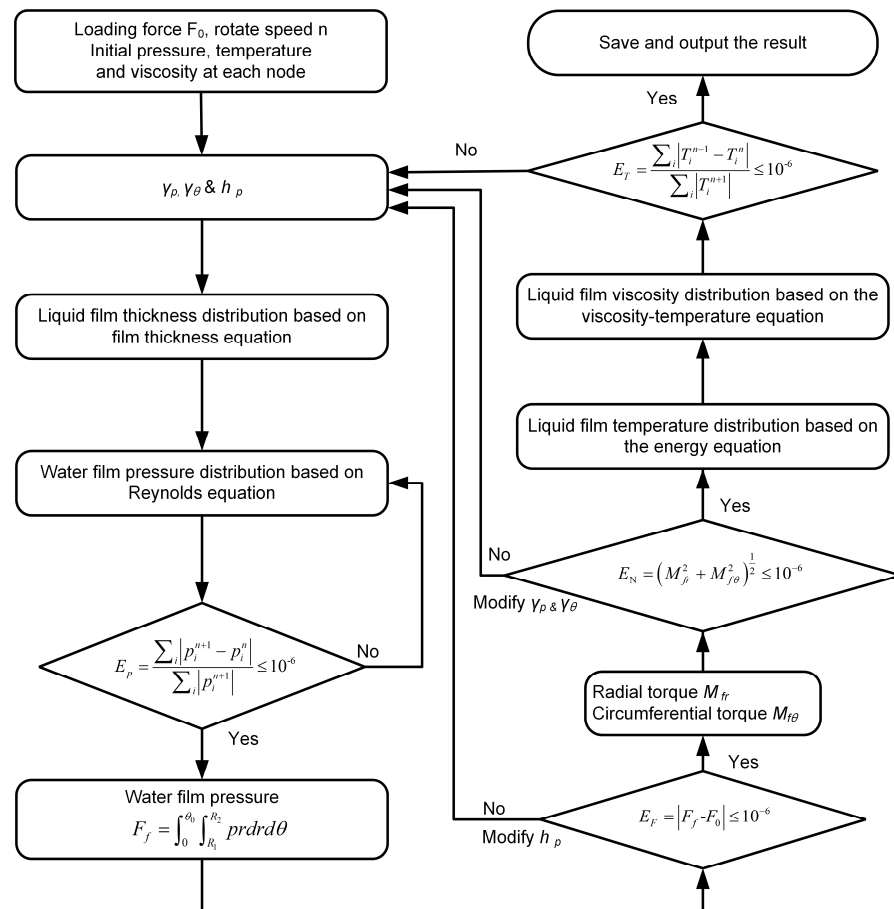


Figure 7. Calculation flow chart.

### 3.4. Model Validation

The simulation concerning the lubrication performance of the bearing in the literature was carried out, and the accuracy of the thermal–hydrodynamic (THD) model was verified [13]. The temperature characteristics of the film under the specific pressure of 0.5–1.5 MPa and the rotational speed of 1200–2500 r/min are shown in Table 1. At the bearing fulcrum, the relative change rate of this model’s temperature is close to the experimental results in the literature, which shows that the model established in this work can predict the lubrication performance of the thrust bearing.

**Table 1.** Comparison of the Literature Data and Model Calculations.

Payloads MPa	Speed r/min	Comparison Value °C	Model Value °C	Relative Rate of Change
0.5	1200	52.38	52.88	0.95%
	1800	54.69	54.84	0.26%
	2500	56.46	56.58	0.20%
1	1200	53.46	53.85	0.72%
	1800	56.38	56.10	−0.51%
	2500	59.23	58.04	−2.01%
1.5	1200	55.38	55.14	−0.44%
	1800	57.69	57.77	0.13%
	2500	60.77	59.96	−1.33%

#### 4. Prediction of Thrust Bearing Lubrication Performance

The ship's tilting-pad thrust bearing was taken as the research object, combined with the emulsification physical parameter equation. To realize the prediction of lubrication performance, a lubrication performance simulation of the thrust bearing was performed, under the mixed emulsification of lubricating oil and seawater in the cruise condition, with a speed of 884 r/min and a load of 6.7 kN. The design parameters of the thrust bearing are shown in Table 2.

**Table 2.** Bearing shingle parameters.

Parameters	Value
Inner diameter, mm	89
Outer diameter, mm	178
Pad angle, deg	36
Thickness of pad, mm	3
Pivot type	spherical
Pivot diameter, mm	135
Pivot angle, °	21.5
Number of pads	8
Thermal conductivity, W/(m K)	47
Inlet temperature/°C	35
Load, kN	6.7
Rotate speed, r/min	884

#### *Effect of Emulsification on the Lubricating Properties of Thrust Bearings*

The lubrication performance of a thrust bearing under mixed emulsification of lubricating oil and seawater was analyzed from four aspects: friction power consumption, film temperature, film pressure, and film thickness, as shown in Figures 8–11. Combined with the emulsification viscosity equation, considering the W/O manifold, phase transition interval and O/W manifold, the performance parameters corresponding to the four groups of moisture content of 0%, 50%, 60% and 100% were analyzed in detail.

Figure 8 is the friction power consumption diagram for different moisture content. One of the main reasons for friction power consumption in bearing hydrodynamic lubrication is viscosity. Therefore, under the condition of constant speed load, the changing trend of bearing friction power consumption is similar to that of viscosity in different moisture content (Figure 6). Compared to the friction power consumption of 0% moisture content (oil state), the friction coefficient of 50%, 60%, and 100% moisture content (seawater) changed by 111.8%, −70.2% and −90.5%, respectively. Under the W/O manifold, seawater pollution will increase the bearing friction loss, increase the load of the driving device, and reduce the driving efficiency.

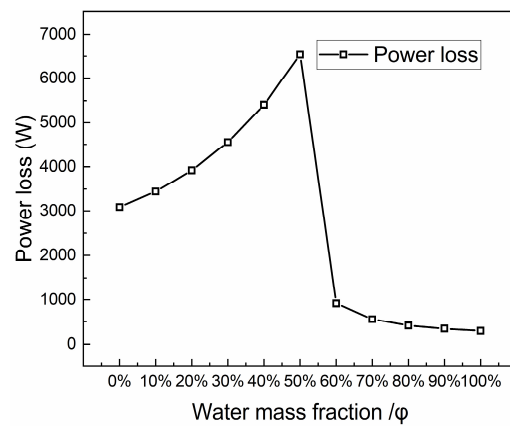


Figure 8. Friction power consumption of different moisture content.

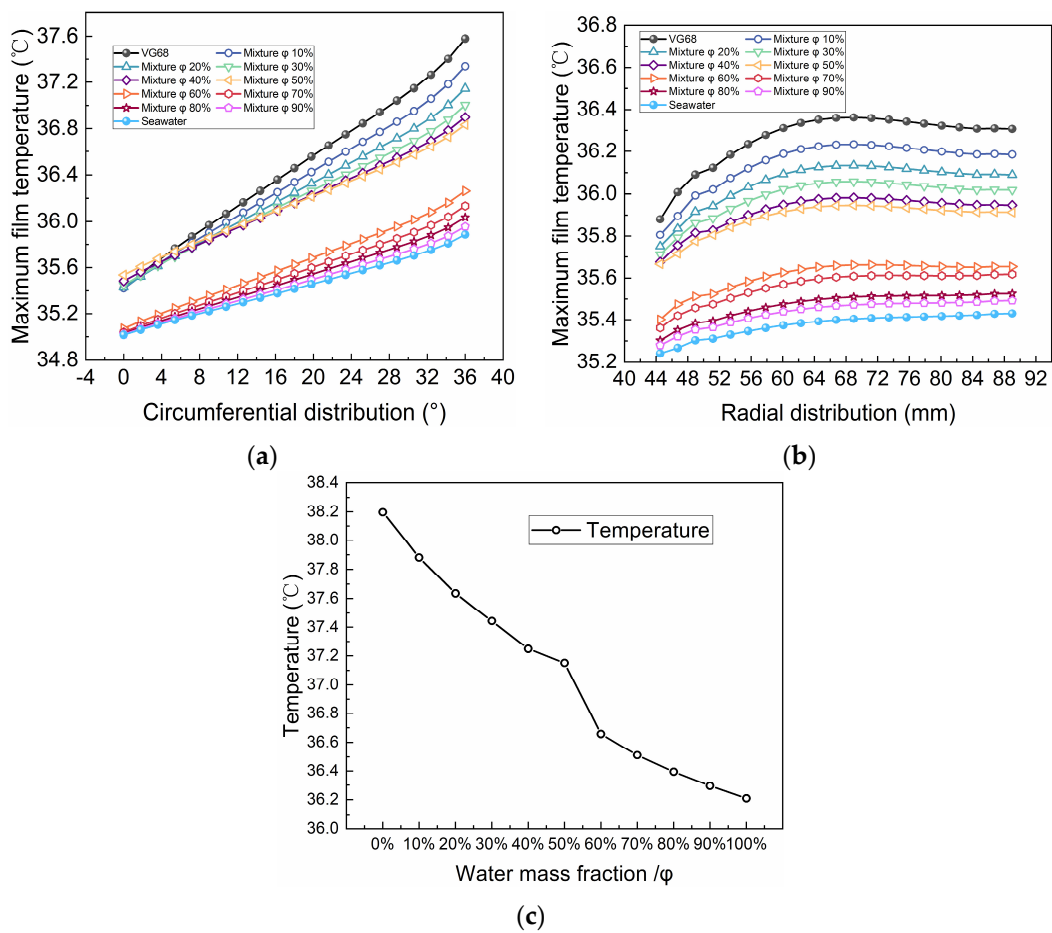
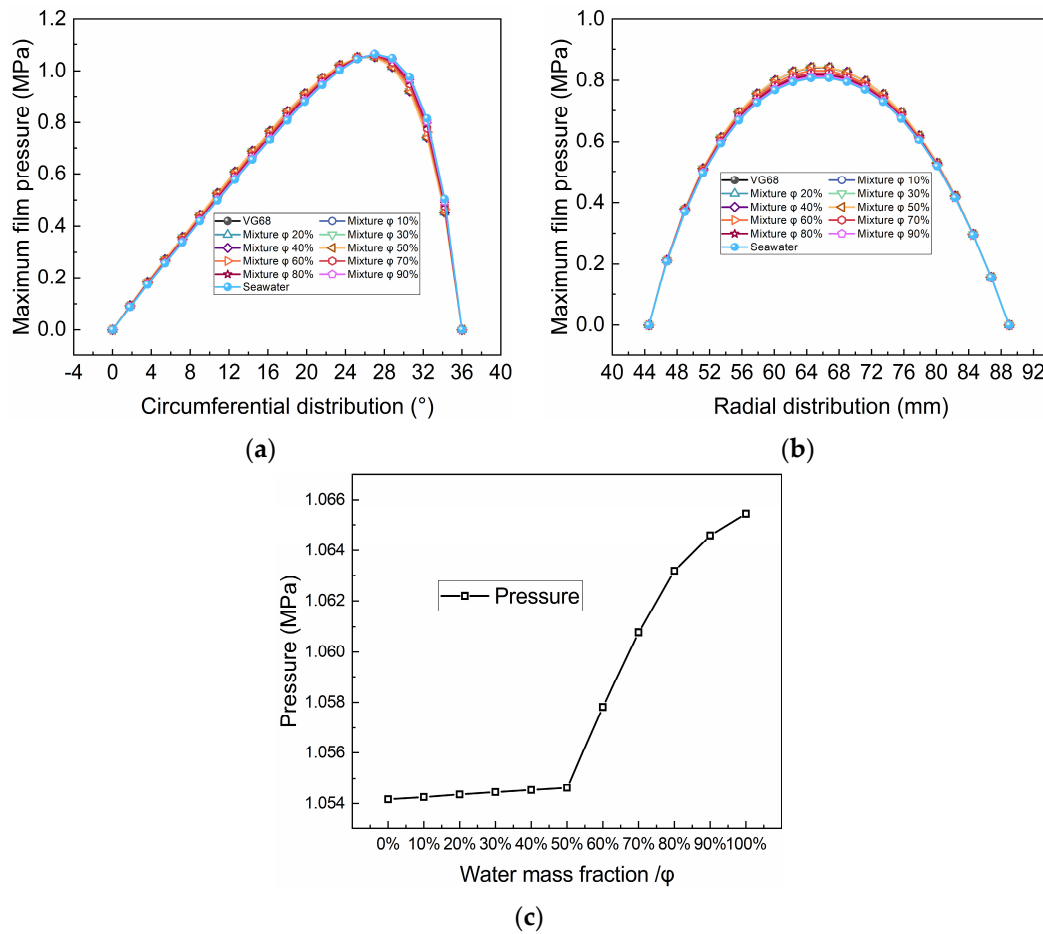


Figure 9. Membrane temperature characteristics for different moisture content: (a) circumferential distribution of temperature; (b) radial distribution of temperature; (c) maximum film temperature.



**Figure 10.** The film pressure characteristics for different moisture content: (a) circumferential pressure distribution; (b) radial pressure distribution; (c) maximum pressure.

An increase in bearing friction power consumption will cause an increase in heat, thereby causing a change in film temperature. Film temperature is shown in Figure 9. The amplitudes of the circumferential centerline temperature of the pad from the inlet ( $0^\circ$ ) to the outlet ( $36^\circ$ ) (Figure 9a), and the radial centerline temperature of the pad from the inner diameter (44.5 mm) to the outer diameter (89 mm) (Figure 9b) gradually decreases. The amplitude changes greatly in the range of 50–60%, reaching  $-85.9\%$  at the maximum temperature point of the pad (Figure 9c). Because seawater increases the specific heat capacity of the lubricating oil, the heat transfer capacity of the liquid per unit mass increases, resulting in an increase in friction power consumption and no dramatic temperature rise of the film. In Figure 9a, the inlet temperature of 0–50% moisture content increases with the increase in moisture content, which is due to the increase in friction power consumption, increasing cyclic temperature between pads. Under the combined effect of specific heat capacity, the inlet temperature change rate is only 0.3%.

Figure 10 is the pressure change diagram of the bearing with different moisture content. The pressure is relatively stable with a moisture content of 0–50%, and the maximum pressure (see Figure 10c) increases by 1.1% with a moisture content of 60–100%. The pressure distribution of the film on the pad with a moisture content of 60–100% in Figure 10a,b is as follows: in the circumferential distribution of pressure, the pressure peak amplitude increases, the angle increases, and the curve becomes steeper. The pressure peak amplitude in the radial distribution of pressure is reduced by 4.0%. Therefore, it can be judged that in a lubricating environment with a continuous water phase, the pressure peak of the pad has a circumferential shift. The decrease in amplitude of the radial distribution

is due to the increase in amplitude of the circumferential distribution and the offset of the pressure peak to the outlet direction.

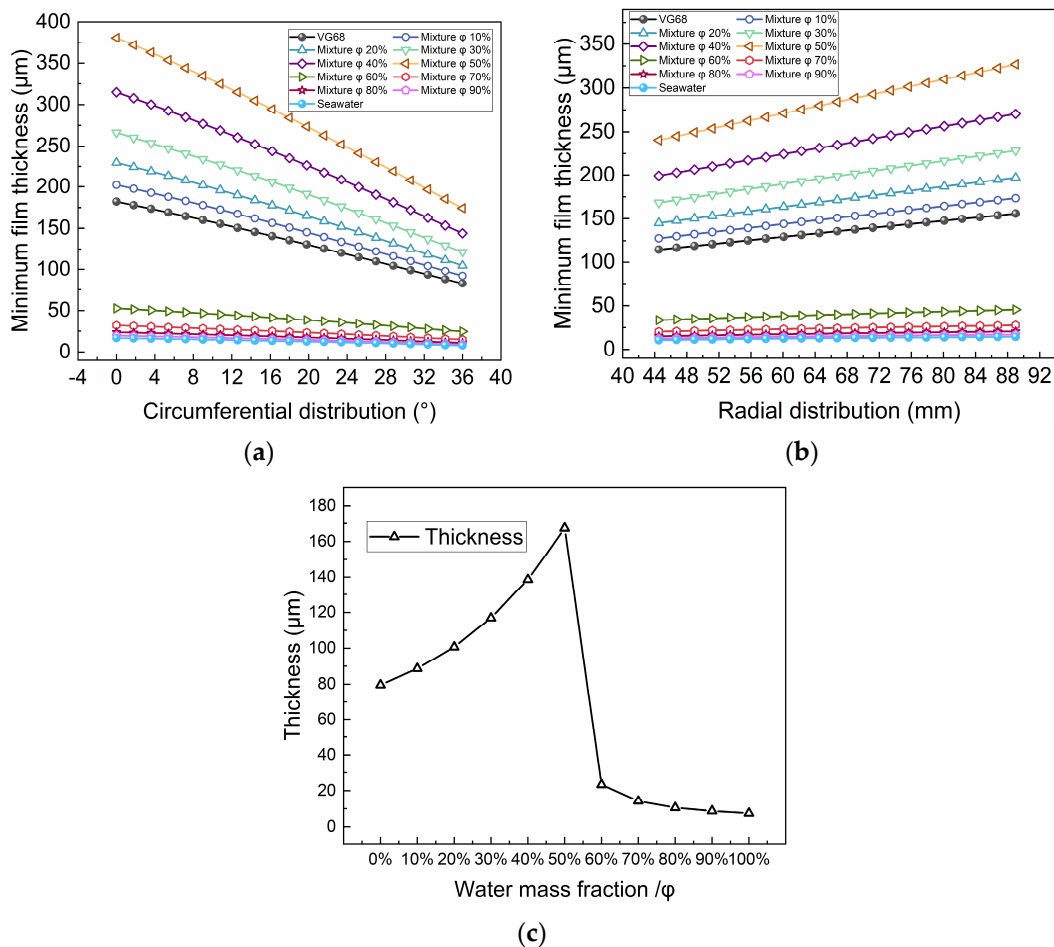


**Figure 11.** Film thickness characteristics for different moisture content: (a) circumferential film thickness distribution; (b) radial film thickness distribution; (c) minimum film thickness.

The change of film thickness distribution in a moisture content range of 0–100% is shown in Figure 11a,b. The film thickness decreases gradually from the inlet to the outlet, and from the outer diameter to the inner diameter. With the increase in moisture content, the distribution of film thickness in the W/O manifold gradually becomes steeper, while the distribution of film thickness in the O/W manifold gradually becomes gentler. The variation of the minimum film thickness in Figure 11c is similar to that of the viscosity. For the specific moisture content of 0%, the minimum film thickness of 50%, 60%, and 100% (seawater) changed by 110.3%,  $-70.6\%$ , and  $-90.6\%$ , respectively. The minimum film thickness at 50% moisture content is more than 7 times that at 60% moisture content. Therefore, in the process of a damaged ship returning to port, once the moisture content exceeds the limit, the bearing lubrication medium will undergo demulsification. Because the loss of film thickness is greater than the steady-state film thickness after demulsification, this may lead to impact between the bearing and the inference disc. In addition, under the O/W manifold, the minimum thickness of the film decreases from 23.4  $\mu\text{m}$  to 7.4  $\mu\text{m}$ . According to the theory of mixed and boundary lubrication [38], mixed lubrication or boundary lubrication occurs when the ratio of film thickness to comprehensive pad roughness is less than three. Considering that ship bearings will produce local wear or particles equivalent to the thickness of the film during service [39,40] if the local roughness of the pad reaches 2.5–7.8, continuous mixed friction may occur, damaging the pad and even causing bearing damage.

## 5. Conclusions

The prediction model of lubrication performance needs to be established for the working state of ship thrust-bearing oil when it is polluted by seawater. In this study, the emulsified viscosity characterization test of ship lubricating oil mixed with seawater was carried out, and the viscosity curves under different moisture content and temperature conditions were fitted. A THD bearing lubrication model considering the emulsified viscosity equation was built, and the FDM method was used to calculate the thrust bearing lubrication characteristics under seawater pollution. The conclusions are as follows:

- (1) Under light load conditions, white metal bearings can work in an oil–water mixed environment with varying moisture content. In lubrication environments of a mixed liquid manifold caused by varying moisture content, the bearing lubrication performance is different. The bearing lubrication state is better in the W/O manifold with less than 50% moisture content than in the O/W manifold with more than 60% moisture content.
- (2) After oil is polluted by seawater, the viscosity and specific heat capacity of the physical parameters have a significant effect on the lubrication performance of the bearing. The change in viscosity affects the friction power consumption, film thickness, local film pressure, and film temperature of the bearing. The specific heat change mainly affects the film temperature, and the higher the moisture content, the lower the film temperature.
- (3) In the W/O manifold, seawater pollution increases the power loss of the bearing and increases the thickness of the film. In the short term, our study shows the minimum film thickness increased by 110.3% and the bearing obtains better bearing capacity. In the O/W manifold, the film thickness is only 23.4–7.4  $\mu\text{m}$ , and the pressure peak will shift to the direction of the pad outlet with the increase in moisture content.
- (4) It is particularly important to note that in the demulsification stage, the viscosity of the oil–water mixture suddenly changes, and the reduction of film thickness will be more than six times that of the film thickness in the O/W manifold, which may lead to bearing wear or even impact. In addition, the local roughness of the pad in the W/O manifold is greater than 2.5–7.8, or there are particles of the same size in the lubricating fluid, which increases the probability of mixed lubrication of the bearing. Therefore, it is necessary to monitor the manifold characteristics of the bearing lubricant during the ship's return to port to prevent bearing accidents in the short term.
- (5) This work only considered light load conditions. To study the bearing performance under worse working conditions, more viscosity tests and bearing tests need to be carried out to correct and verify the correctness of the model.

**Author Contributions:** Conceptualization, W.O. and X.Z.; methodology, J.H.; software, B.W.; validation, Z.Y., W.O. and B.W.; formal analysis, Z.Y.; investigation, B.L.; resources, B.L.; data curation, W.O.; writing—original draft preparation, Z.Y.; writing—review and editing, W.O.; visualization, Z.Y.; supervision, X.Z.; project administration, B.L.; funding acquisition, B.L. All authors have read and agreed to the published version of the manuscript.

**Funding:** This work was financially supported by the National Natural Science Foundation of China (grant numbers 52071244 and 52101370) and the Natural Science Foundation of Hubei Province of China (No. 2023AFA098).

**Data Availability Statement:** Data are available upon request from the authors.

**Acknowledgments:** The authors are so grateful for the valuable suggestions from Minjie Zhu during the study.

**Conflicts of Interest:** The authors declare that they have no known competing financial interests or personal relationships that could have appeared to influence the work reported in this paper.

## Nomenclature

$t$	Temperature (°C)
$n, m$	Viscosity parameters of Walther's model
$c_1, c_2$	Emulsified oil viscosity influence parameters
$A, B, C$	Viscosity parameters of Vogel's model.
$\mu$	Dynamic viscosity (mPas)
$\mu_c$	Viscosity of the continuous phase (mPas)
$\mu_d$	Viscosity of the dispersed phase (mPas)
$\mu_r$	Viscosity ratio after mixing
$\varphi$	Moisture content
$\varphi_c$	Moisture content of turning point
$r, \theta, z$	Cylindrical coordinates (m, rad, m)
$P$	Pivot
$R_1$	Inner radius of pad (mm)
$R_2$	Outer radius of pad (mm)
$r_p$	Pivot radius (rad)
$\theta_p$	Pivot angle (rad)
$\theta_0$	Pad angle (rad)
$\gamma_r$	Radial tilt angle of the pad (rad)
$\gamma_\theta$	Circumferential tilt angle of the pad (rad)
$h$	Film thickness ( $\mu\text{m}$ )
$h_p$	Film thickness at the pivot ( $\mu\text{m}$ )
$n$	Rotate speed (r/min)
$\omega$	Angular velocity (rad/s)
$p$	Film pressure (MPa)
$\Gamma$	Periphery boundary
$\Gamma_1$	Film rupture boundary
$\rho$	Density ( $\text{Kg}/\text{m}^3$ )
$\rho_{mix}$	Mixture density ( $\text{Kg}/\text{m}^3$ )
$\rho_{seawater}$	Seawater density ( $\text{Kg}/\text{m}^3$ )
$\rho_{oil}$	Oil density ( $\text{Kg}/\text{m}^3$ )
$C_p$	Specific heat at constant pressure ( $\text{J}/(\text{kg}\cdot^\circ\text{C})$ )
$C_{mix}$	Mixing specific heat ( $\text{J}/(\text{kg}\cdot^\circ\text{C})$ )
$C_{seawater}$	Seawater specific heat ( $\text{J}/(\text{kg}\cdot^\circ\text{C})$ )
$C_{oil}$	Oil specific heat ( $\text{J}/(\text{kg}\cdot^\circ\text{C})$ )
$k$	Heat transfer coefficient ( $\text{W}/(\text{m}\cdot\text{K})$ )
$t_{in}$	Inlet temperature (°C)
$\lambda$	Convection coefficient ( $\text{W}/(\text{m}^2\cdot\text{K})$ )
$k_b$	Boundary heat transfer coefficient ( $\text{W}/(\text{m}\cdot\text{K})$ )
$T_b$	Boundary temperature (°C)
$\Delta T$	Solid–liquid boundary temperature difference (°C)
$E_p$	Pressure convergence criteria
$E_T$	Temperature convergence criteria
$E_F$	Force criteria
$E_N$	Moment criteria
$M_{fr}$	The radial direction torque (Nm)
$M_{f\theta}$	The circumferential direction torque (Nm)
$F_0$	Loading force (N)
$F_f$	Total film force (N)

## References

1. Dadouche, A.; Conlon, M.J. Operational performance of textured journal bearings lubricated with a contaminated fluid. *Tribol. Int.* **2016**, *93*, 377–389. [[CrossRef](#)]
2. Khonsari, M.; Pascovici, M.; Kucinski, B. On the scuffing failure of hydrodynamic bearings in the presence of an abrasive contaminant. *J. Tribol.* **1999**, *121*, 90–96. [[CrossRef](#)]
3. Cantley, R.E. The effect of water in lubricating oil on bearing fatigue life. *ASLE Trans.* **1977**, *20*, 244–248. [[CrossRef](#)]

4. Harika, E.; Bouyer, J.; Fillon, M.; Hélène, M. Effects of water contamination of lubricants on hydrodynamic lubrication: Rheological and thermal modeling. *J. Tribol.* **2013**, *135*, 041707. [[CrossRef](#)]
5. Bloch, H. Criteria for water removal from mechanical drive steam turbine lube oils. *Lubr. Eng.* **1980**, *36*, 699–707.
6. Hamaguchi, H.; Spikes, H.; Cameron, A. Elastohydrodynamic properties of water in oil emulsions. *Wear* **1977**, *43*, 17–24. [[CrossRef](#)]
7. Zhang, F.; Fillot, N.; Bouscharain, N.; Devaux, N.; Philippon, D.; Matta, C.; Morales-Espejel, G.E. Water droplets in oil at the inlet of an EHD contact: A dual experimental and numerical investigation. *Tribol. Int.* **2023**, *177*, 108015. [[CrossRef](#)]
8. Hili, J.; Pelletier, C.; Jacobs, L.; Olver, A.; Reddyhoff, T. High-Speed Elastohydrodynamic Lubrication by a Dilute Oil-in-Water Emulsion. *Tribol. Trans.* **2018**, *61*, 287–294. [[CrossRef](#)]
9. Soltanahmadi, S.; Morina, A.; van Eijk, M.C.; Nedelcu, I.; Neville, A. Tribochemical study of micropitting in tribocorrosive lubricated contacts: The influence of water and relative humidity. *Tribol. Int.* **2017**, *107*, 184–198. [[CrossRef](#)]
10. Haque, T.; Korres, S.; Carey, J.T.; Jacobs, P.W.; Loos, J.; Franke, J. Lubricant effects on white etching cracking failures in thrust bearing rig tests. *Tribol. Trans.* **2018**, *61*, 979–990. [[CrossRef](#)]
11. Liu, H.; Xu, H.; Zhang, Y.; Ji, H.; Ge, Y.; Ellison, P.; Jin, Z. The influence of sea water in oil emulsion on bearing performance. *Proc. Inst. Mech. Eng. Part J J. Eng. Tribol.* **2009**, *223*, 457–468. [[CrossRef](#)]
12. Harika, E.; Jarny, S.; Monnet, P.; Bouyer, J.; Fillon, M. Effect of water pollution on rheological properties of lubricating oil. *Appl. Rheol.* **2011**, *21*, 12613.
13. Almqvist, T.; Glavatskikh, S.B.; Larsson, R. THD Analysis of Tilting Pad Thrust Bearings—Comparison Between Theory and Experiments. *J. Tribol.* **2000**, *122*, 412–417. [[CrossRef](#)]
14. Ismail, A.S.I.; Ismail, I.; Zoveidavianpoor, M.; Mohsin, R.; Piroozian, A.; Misnan, M.S.; Sariman, M.Z. Review of oil–water through pipes. *Flow Meas. Instrum.* **2015**, *45*, 357–374. [[CrossRef](#)]
15. Prashad, H. A study of electrical pitting of journal bearings with water-contaminated lubricant. *Tribotest* **2000**, *7*, 115–124. [[CrossRef](#)]
16. Trallero, J.L. *Oil-Water Flow Patterns in Horizontal Pipes*; The University of Tulsa: Tulsa, OK, USA, 1995.
17. Ma, J.; Yao, M.; Yang, Y.; Zhang, X. Comprehensive review on stability and demulsification of unconventional heavy oil-water emulsions. *J. Mol. Liq.* **2022**, *350*, 118510. [[CrossRef](#)]
18. Wang, W.; Liu, J.; Wang, P.; Duan, J.; Gong, J. Evolution of dispersed drops during the mixing of mineral oil and water phases in a stirring tank. *Chem. Eng. Sci.* **2013**, *91*, 173–179. [[CrossRef](#)]
19. Rønningsen, H.P. Correlations for predicting Viscosity of W/O-Emulsions based on North Sea Crude Oils. In Proceedings of the SPE International Symposium on Oilfield Chemistry, San Antonio, TX, USA, 14–17 February 1995.
20. Nädler, M.; Mewes, D. Flow induced emulsification in the flow of two immiscible liquids in horizontal pipes. *Int. J. Multiph. Flow* **1997**, *23*, 55–68. [[CrossRef](#)]
21. Hu, B.; Angeli, P.; Matar, O.K.; Hewitt, G.F. Prediction of phase inversion in agitated vessels using a two-region model. *Chem. Eng. Sci.* **2005**, *60*, 3487–3495. [[CrossRef](#)]
22. Piela, K.; Delfos, R.; Ooms, G.; Westerweel, J.; Oliemans, R.; Mudde, R. Experimental investigation of phase inversion in an oil–water flow through a horizontal pipe loop. *Int. J. Multiph. Flow* **2006**, *32*, 1087–1099. [[CrossRef](#)]
23. Einstein, A. *Eine Neue Bestimmung der Moleküldimensionen*; ETH Zurich: Montreal, QC, Canada, 1905.
24. Brinkman, H.C. The viscosity of concentrated suspensions and solutions. *J. Chem. Phys.* **1952**, *20*, 571. [[CrossRef](#)]
25. Mooney, M. The viscosity of a concentrated suspension of spherical particles. *J. Colloid Sci.* **1951**, *6*, 162–170. [[CrossRef](#)]
26. Pal, R. Novel viscosity equations for emulsions of two immiscible liquids. *J. Rheol.* **2001**, *45*, 509–520. [[CrossRef](#)]
27. Pal, R. Viscosity–concentration equation for emulsions of nearly spherical droplets. *J. Colloid Interface Sci.* **2000**, *231*, 168–175. [[CrossRef](#)]
28. Ramos-Pallares, F.; Lin, H.; Yarranton, H.W.; Taylor, S.D. Prediction of the liquid viscosity of characterized crude oils by use of the generalized Walther model. *SPE J.* **2017**, *22*, 1487–1505. [[CrossRef](#)]
29. Yuan, W.; Hansen, A.; Zhang, Q. Predicting the temperature dependent viscosity of biodiesel fuels. *Fuel* **2009**, *88*, 1120–1126. [[CrossRef](#)]
30. Testing, A.S.F. Materials. In *Standard Practice for the Preparation of Substitute Ocean Water*; ASTM International: West Conshohocken, PA, USA, 2013.
31. Mendoza, C.I.; Santamaría-Holek, I. Improved viscosity-concentration equation for emulsions of nearly spherical droplets. *arXiv* **2009**, arXiv:0903.5507.
32. Pak, B.C.; Cho, Y.I. Hydrodynamic and heat transfer study of dispersed fluids with submicron metallic oxide particles. *Exp. Heat Transf. Int. J.* **1998**, *11*, 151–170. [[CrossRef](#)]
33. Mukhaimer, A.; Al-Sarkhi, A.; El Nakla, M.; Ahmed, W.; Al-Hadhrami, L. Pressure drop and flow pattern of oil–water flow for low viscosity oils: Role of mixture viscosity. *Int. J. Multiph. Flow* **2015**, *73*, 90–96. [[CrossRef](#)]
34. Masaaki Miyatake, S.Y. Numerical investigation of static and dynamic characteristics of aerostatic thrust bearings with small feed holes. *Tribol. Int.* **2010**, *43*, 1353–1359. [[CrossRef](#)]
35. Uichiro Nishio, K.S.; Yoshimoto, S. Numerical calculation and experimental verification of static and dynamic characteristics of aerostatic thrust bearings with small feedholes. *Tribol. Int.* **2011**, *44*, 1790–1795. [[CrossRef](#)]

36. Chen, R.; Han, Q.; Wang, X.; Cui, Y.; Liu, K. Performance Research on Bi-directional Tilting Pad Thrust Bearing Considering the Verticality Error of Thrust Plate. *J. Phys. Conf. Ser.* **2020**, *1634*, 012155. [[CrossRef](#)]
37. Wang, B.; Ouyang, W.; Wang, S.T.; Sheng, C.X.; Xiao, J.H.; Li, Z. Dynamic Model and Parameter Identification of Magnetic Liquid-Double-Suspension Elastic-Supported Thrust Bearing. *Int. J. Struct. Stab. Dyn.* **2023**, *23*, 2350033. [[CrossRef](#)]
38. Guo, X.; Han, Y.; Chen, R.; Jiayu, W.; Xiaokang, N. A numerical method to investigate the mixed lubrication performances of journal-thrust coupled bearings. *Ind. Lubr. Tribol.* **2019**, *71*, 1099–1107.
39. Ronen, A.; Malkin, S. Wear mechanisms of statically loaded hydrodynamic bearings by contaminant abrasive particles. *Wear* **1981**, *68*, 371–389. [[CrossRef](#)]
40. Begelinger, A.; De Gee, A. Abrasive wear of bearing materials—A comparison of test methods. *Wear* **1985**, *101*, 141–154. [[CrossRef](#)]

**Disclaimer/Publisher’s Note:** The statements, opinions and data contained in all publications are solely those of the individual author(s) and contributor(s) and not of MDPI and/or the editor(s). MDPI and/or the editor(s) disclaim responsibility for any injury to people or property resulting from any ideas, methods, instructions or products referred to in the content.